ADVANCED MATERIALS
www.advmat.de

Tuning Solute-Redistribution Dynamics for Scalable Fabrication of Colloidal Quantum-Dot Optoelectronics

Min-Jae Choi, YongJoo Kim, Hunhee Lim, Erkki Alarousu, Aniruddha Adhikari, Basamat S. Shaheen, Yong Ho Kim, Omar F. Mohammed, Edward. H. Sargent, Jin Young Kim, and Yeon Sik Jung**

Solution-processed colloidal quantum dots (CQDs) are attractive materials for the realization of low-cost and efficient optoelectronic devices. Although impressive CQD-solar-cell performance has been achieved, the fabrication of CQD films is still limited to laboratory-scale small areas because of the complicated deposition of CQD inks. Large-area, uniform deposition of lead sulfide (PbS) CQD inks is successfully realized for photovoltaic device applications by engineering the solute redistribution of CQD droplets. It is shown experimentally and theoretically that the solute-redistribution dynamics of CQD droplets are highly dependent on the movement of the contact line and on the evaporation kinetics of the solvent. By lowering the friction constant of the contact line and increasing the evaporation rate of the droplets, a uniform deposition of CQD ink in length and width over large areas is realized. By utilizing a spray-coating process, large-area (up to 100 cm^2) CQD films are fabricated with 3–7% thickness variation on various substrates including glass, indium tin oxide glass, and polyethylene terephthalate. Furthermore, scalable fabrication of CQD solar cells is demonstrated with 100 cm^2 CQD films which exhibits a notably high efficiency of 8.10%.

Solution-processed colloidal quantum dots (CQDs) are a promising class of semiconducting materials in view of their tunable optical and electronic properties through the quantum size effect.[1–5] They have been used to fabricate next-generation thin-film optoelectronic devices including light-emitting diodes,[6] photodetectors,[7] and solar cells.[8–13] For example, recent perovskite quantum dot-based light-emitting devices showed an external quantum efficiency exceeding 20%.[14–17] Solar cells based on lead chalcogenide CQDs have demonstrated power conversion efficiencies (PCE) of 11.3%[18] and a stabilized output over 150 days when stored in air even without encapsulation,[19] making them candidates for low-cost, stable, and scalable next-generation photovoltaics.

While the performance of CQD solar cells has improved rapidly, the fabrication process is still limited to lab-scale, batch-processing methods, mainly due to reliance on a complex and wasteful multistep layer-by-layer (LbL) ligand exchange method,[20] which to date has been most commonly combined with repeated spin-casting deposition. To overcome this limitation, a solution-phase ligand exchange method was recently developed to realize the single-step fabrication of CQD films.[21–23] In particular, inorganic anions such as metal chalcogenide complexes, halides, and metal-free ions (S^{2-}, OH^-, SCN^-, etc.) have been successfully applied as capping ligands and improved the colloidal dispersion. However, CQDs capped with anions—CQD inks—are typically dispersed in high-boiling-point solvents such as *N*,*N*-dimethylformamide (DMF) or *N*-methylformamide (MFA), which adds complexity to the production of sufficiently thick CQD films.[24] To produce CQD films directly from CQD inks, various approaches have been demonstrated, including centrifugal casting[7] and supersonic spray coating.[25] However, so far, these methods have been limited in scale to batch-processing; large-scale, single-step QD film formation has not yet been realized.

One of the main challenges when forming films from CQD inks is to inhibit (or even control) the spatial redistribution of the dispersed solute during late-state evaporation.[26] This redistribution often results in poorly controlled film morphology

Dr. M.-J. Choi, H. Lim, Dr. Y. H. Kim, Prof. Y. S. Jung
Department of Materials Science and Engineering
Korea Advanced Institute of Science and Technology (KAIST)
291 Daehak-ro, Yuseong-gu, Daejeon 34141, South Korea
E-mail: ysjung@kaist.ac.kr
Dr. M.-J. Choi, Prof. E. H. Sargent
Department of Electrical and Computer Engineering
University of Toronto
10 King's College Road, Toronto, Ontario M5S 3G4, Canada
Dr. Y. Kim, Prof. Y. S. Jung
Institute for NanoCentury
Korea Advanced Institute of Science and Technology
291 Daehak-ro, Yuseong-gu, Daejeon 34141, South Korea
Dr. E. Alarousu, Dr. A. Adhikari, B. S. Shaheen, Prof. O. F. Mohammed
King Abdullah University of Science and Technology (KAUST)
Thuwal 23955-6900, Kingdom of Saudi Arabia
Dr. J. Y. Kim
Fuel Cell Research Center
Korea Institute of Science and Technology
Seoul 02792, South Korea
E-mail: jinykim@kist.re.kr
The ORCID identification number(s) for the author(s) of this article can be found under https://doi.org/10.1002/adma.201805886.

DOI: 10.1002/adma.201805886

and is detrimental to optoelectronic device performance.[27–29] Although the mechanism for drying of droplets is well established on microsized colloidal particles such as silica and PMMA,[30–33] there have been only a few studies on the deposition pattern of CQD droplets,[34,35] especially for CQD inks. Nonetheless, understanding the redistribution of CQDs during the drying is critical for large-scale solution-casting such as blade coating, roll-to-roll printing, inkjet printing, and spray deposition.

Here we report the fabrication of uniform, large-area PbS CQD films of 100 cm^2 area by tuning the deposition patterns of ultrasonic-generated fine CQD droplets. We show experimentally that the redistribution dynamics of CQDs is highly dependent on the movement of the solid–liquid–vapor contact line and evaporation kinetics of the solvent—findings further supported by a theoretical model. By lowering the friction constant of the contact line and increasing the evaporation rate of the droplets, we achieve uniform and scalable deposition of CQD inks. We demonstrate the versatility of the method using three types of iodide-capped CQD inks deposited on a variety of substrates. The resultant CQD films exhibit much lower surface roughness and reduced charge carrier recombination compared to that of CQD films fabricated by the conventional LbL method. To our knowledge, this is the first report of engineering the deposition dynamics of CQD inks and the demonstration of centimeter-scale large-area fabrication of CQD films.

We began from solution-phase ligand exchange to produce CQD inks, exhibiting electronically conductive property when they are deposited. Iodide ligands such as methylammonium iodide (MAI), methylammonium lead triiodide ($MAPbI_3$), and lead iodide (PbI_2) are good candidates for solution-phase ligand exchange due to their excellent performance when applied to CQD solar cells to date.[18,28] Therefore we exchanged oleic acid (OA) ligands of CQDs with MAI ligands. The MAI-capped CQD inks were well stabilized in DMF due to existence of their surface charge, which is confirmed by zeta potential value of −30 mV, whereas OA-capped CQDs show ≈0 mV (Figure S1, Supporting Information). This is in good agreement with previous literature reporting that iodide-capped CQDs exhibit a negative surface charge while OA-capped CQDs do not have a surface charge.[21,36]

We encountered serious nonuniform problem with deposition of CQD inks at room temperature (RT) which is confirmed by photograph and thickness profiler (**Figure 1**a). During a drying step, most CQDs in the droplet accumulated at the center, creating a micrometer-thick island, whereas only small amounts of CQDs were deposited in other areas. This center-focused island-like pattern away from the periphery of droplet is consistent with the previous reports[29,37] which occurs when the contact line of droplet is mobile. We hypothesized that this center-focused deposition comes from slow drying process, giving CQDs enough time to migrate with solvent rather than be deposited on substrate (Figure 1b). To suppress this migration, we accelerate evaporation of solvent to induce quenching effect during the drying stage. As shown in Figure 1c, we could obtain uniform deposition of CQD inks on a heated substrate at 50 °C, which enables 6.4 times faster evaporation of solvent than evaporation at RT. When the evaporation rate is fast enough, the contact line recedes quickly thus CQDs are deposited on the substrate rather than piled with the receding contact line, resulting in the uniform deposition (Figure 1d). Increasing evaporation rate by varying its surrounding atmosphere (e.g., under vacuum condition; Figure S2, Supporting Information) was also effective to realize uniform deposition of CQD inks.

To fully understand the effect of evaporation rate of droplet on the deposition pattern, we theoretically calculated thickness profiles of solutes for different evaporation rate based on the Onsager principle.[38,39] The deposition pattern of the droplets is largely affected by the friction coefficient, which is the rate of energy dissipated on the moving boundary of the droplets. Different from previous model for pinned contact line,[40] energy dissipation is controlled by extra friction constant of contact line ξ and viscosity of solution η. In this model, time evolution of solute profile is obtained as a function of relative evaporation rate of solvent k_{ev} by minimizing energy dissipation and free energy change rate.[41] Final solute profiles as a function of normalized radial distance from droplet center (r/R) for different evaporation rates k_{ev} of droplet with mobile contact line are shown in Figure 1e. This evaporation-rate dependent solute-distribution trend appears to be consistent for the different size of droplets (Figure S3, Supporting Information). For qualitative comparison with theory, we calculated the term Th/Th_{avg}, from the thickness profiles of the deposition patterns (Figure S4, Supporting Information), where Th is the thickness of the solutes and Th_{avg} is the average thickness of the solutes from center to edge. Figure 1f shows Th/Th_{avg} of deposition of CQD inks as a function of radial distance (r/R) from center of deposition to edge of deposition with different evaporation rate. For slow evaporation (0.42 μL min^{-1}, substrate temperature = RT), big islands formed at the center of the droplet, yielding Th_{max}/Th_{avg} of ≈68, where Th_{max} is the maximum thickness of the deposition. As we expected in calculation, these islands became smaller and shifted toward the edge with an increase in the evaporation rate, and the flatness of the QD films was markedly improved, finally allowing Th/Th_{avg} to approach a value of ≈1 at an evaporation rate of 2.67 μL min^{-1} (substrate temperature = 50 °C). The dependence of the standard deviation (a measure of uniformity) of Th/Th_{avg} on the evaporation rate shows good agreement with the calculation results; a higher evaporation rate enables more uniform deposition of the solutes (Figure S5, Supporting Information). The consistent trend between the calculation (Figure 1e) and the experimental outcome (Figure 1f) with varying evaporation rates confirms the importance of the rapid evaporation of the solvent for the uniform deposition of solutes from colloidal droplets.

The deposition pattern of CQD inks was completely different with that of OA-capped CQDs which shows coffee-ring effect;[40] most CQDs accumulated at the edge only (Figure S6, Supporting Information). The substantially different deposition patterns in OA-capped CQD (coffee-ring) and MAI-capped CQD inks (island-like) can be explained by the difference in the relative friction coefficient of the contact lines, which is proportional to ξ/η.[41] CQD inks showed higher η (Table S1, Supporting Information) and lower ξ (Figure S7, Supporting Information) compared to OA-capped CQDs, resulting in mobile contact line during the drying step while contact line of OA-capped CQDs is strongly pinned. This indicates that

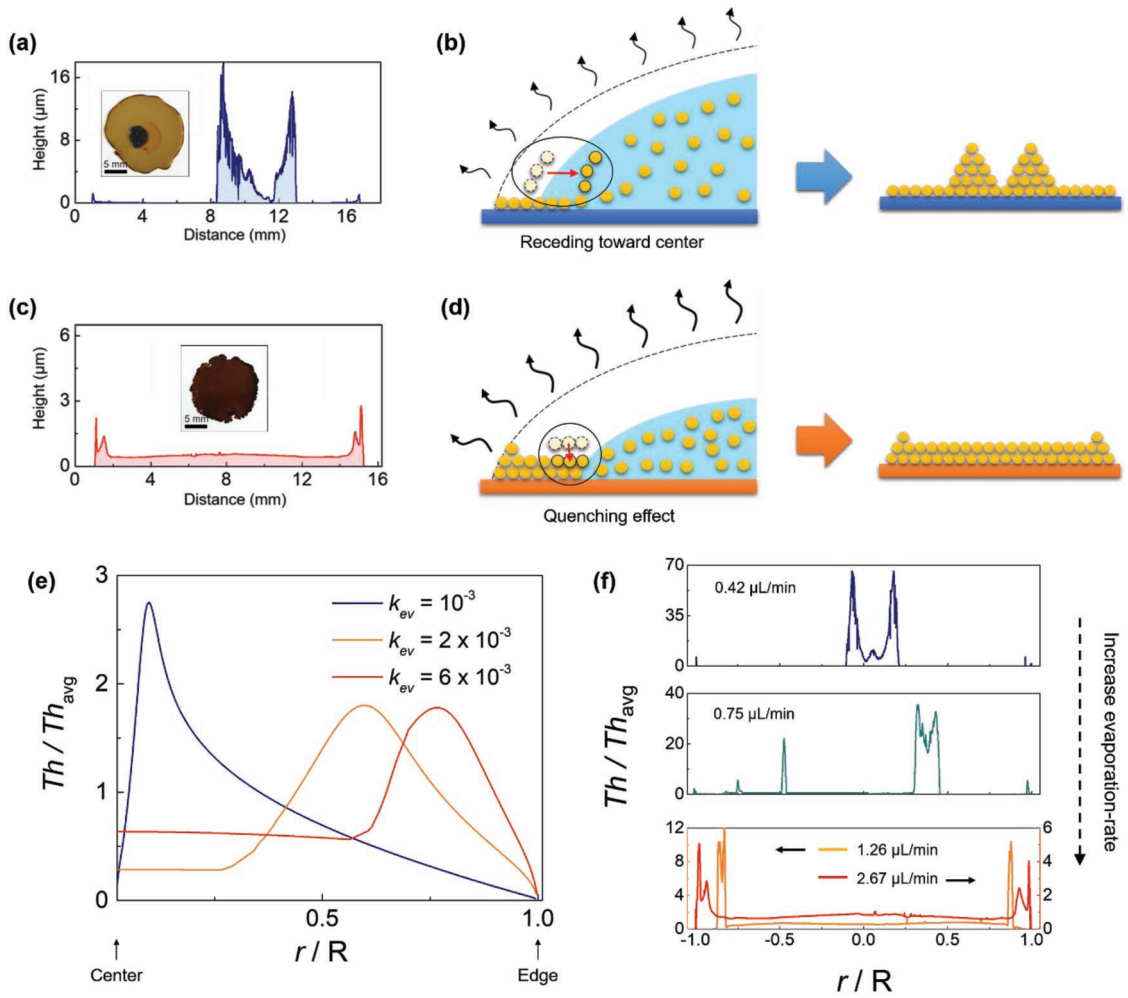

Figure 1. Solute-redistribution dynamics of CQD inks. Photograph, and thickness profiles of the deposition of CQD inks when the substrate temperature is at RT a) and 50 °C c). Schematic illustration of solute (CQD) redistribution when the evaporation rate is slow b), and the evaporation rate is fast d) during the drying process of solution droplet. The dashed line is an initial profile of droplet. Red arrow indicates position change of CQDs. e) Theoretically calculated concentration profiles of CQDs in radial direction for different evaporation rates k_{ev}. Thickness of the solutes (Th) as a function of the distance from the center (r) is normalized by the average thickness from center to edge, Th_{avg}. Evaporation rate is increased to 2×10^{-3} and 6×10^{-3} to mimic the 6-time increased evaporation rate of experimental system for fastest evaporation case at 50 °C. f) Thickness of the deposition of CQD inks, Th, normalized by the average thickness, Th_{avg}, plotted as a function of radial distance, r/R, from the center of droplet for different evaporation rates.

solute-redistribution of droplet is highly dependent on the degree of freedom of contact line during the drying.

We extended this principle to large areas by utilizing an ultrasonic spray-coating system (**Figure 2**a). The nozzle uniformly sprayed numerous microdroplets containing CQDs while it scanned the surface area of the substrate. The sprayed droplets rapidly spread (Figure S8, Supporting Information) on the substrate and merge to one large droplet within a second, whereas evaporation of droplets takes more than a few minutes due to the high boiling point of the solvent. This makes it possible to show the evaporation-rate-dependent CQD-redistribution behavior, which is similar to the case of drop-cast CQD inks, as depicted in Figure 1, i.e., CQD inks accumulated locally when the evaporation rate was low or while more uniform deposition occurred with faster evaporation (Figure S9, Supporting Information). However, a too fast solvent evaporation from spray-coated CQD microdroplets resulted in nonuniform deposition because the drying process ended before the droplets had merged into a uniformly wet film on the substrate.

Under the optimized evaporation-rate conditions we got from Figure S9 (Supporting Information), a uniform single-step spray-coated (SSC) CQD film was successfully obtained. This SSC films were even more uniform compared to the film produced by drop deposition (Figure 1c) because spraying numerous microdroplets over the substrate enables reaching the equilibrium contact angle immediately while drop deposition needs longer time for reaching equilibrium by spreading of droplets (Figure S10, Supporting Information). The area of deposition can be extended easily by controlling the scanning range of the spray-nozzle that large-area (10×10 cm^2) deposition of CQD inks was demonstrated on various substrates including glass, indium tin oxide (ITO) glass, and polyethylene terephthalate (PET) (Figure 2b). It should be noted that the thickness

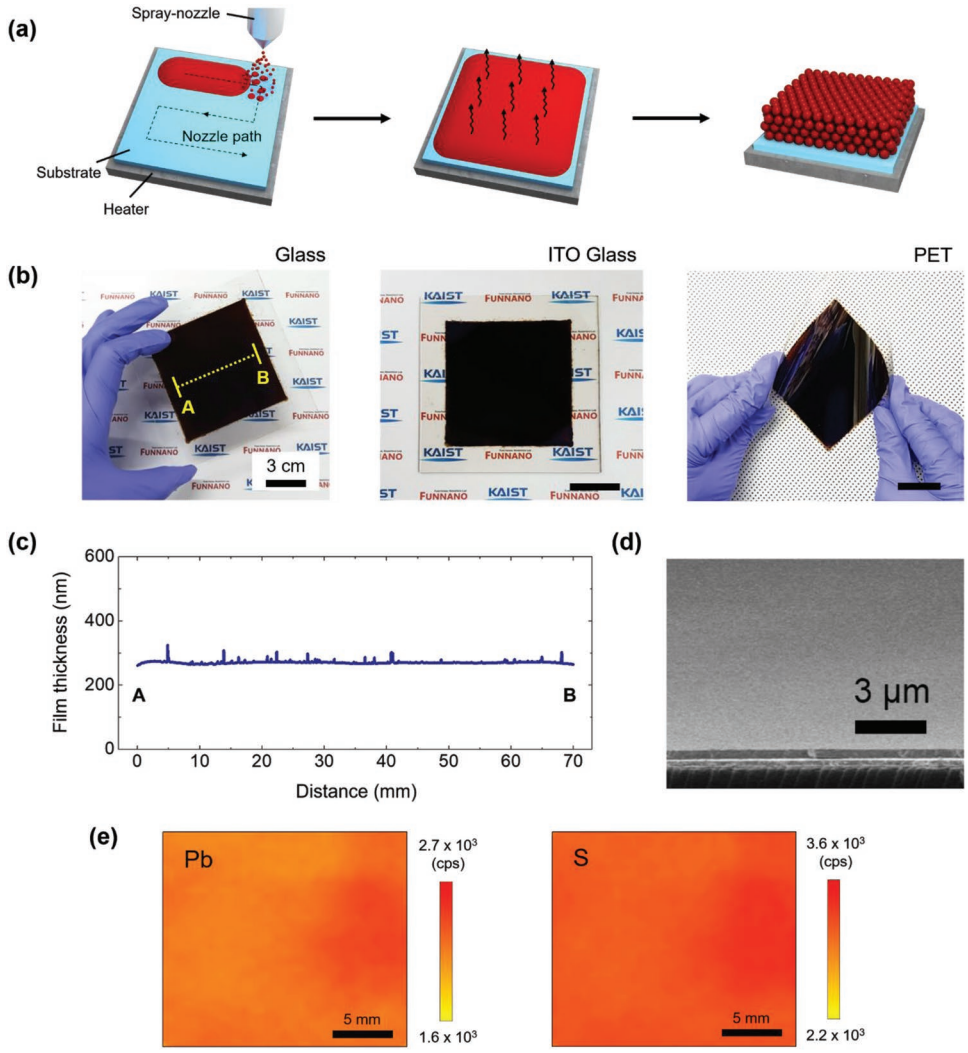

Figure 2. Large-area deposition of CQD inks via single-step spray-coating. a) Scheme of the fabrication process of CQD films by using spray-coating method. b) Photograph of CQD films (10 cm × 10 cm) on a glass substrate, indium tin oxide (ITO) glass substrate, and PET substrate. c) Thickness profile of CQD films on the glass substrate as shown in (b) from "A" to "B". d) Cross-sectional scanning electron microscopy image of CQD films deposited on ITO glass substrate. e) X-ray fluorescence mapping of Pb and S on the CQD film.

uniformity is dependent on the distance between each nozzle path (see more details in Figure S11, Supporting Information).

We quantified the uniformity of the SSC CQD films using a thickness profilometer. Figure 2c shows the thickness profiles of SSC CQD film on the glass substrate as shown in Figure 2b along the line between "A" and "B." It shows maximum variation of 35 nm along the 7 cm line, and root-mean-square roughness values of 11.9 nm—4.2% of the average film thickness, indicative of highly uniform CQD film formation. Cross-sectional scanning electron microscope (SEM) image also supports the crack-free, uniform construction of SSC CQD film (Figure 2d). Because thickness profiling is a 1D analysis method, we additionally carried out X-ray fluorescence (XRF) mapping of the SSC CQD film to characterize their 2D uniformity. The mapping images in Figure 2e indicate that the elements Pb and S were uniformly distributed over the substrate, in good agreement with the afore-shown excellent thickness uniformity of the films. The excitonic features of the PbS CQD inks in the optical absorption spectra were fully preserved following deposition as a solid film (Figure S12, Supporting Information), which indicates that the CQDs have retained their quantum confinement characteristics upon deposition.

The thickness of SSC film was easily controlled from 42 to 304 nm or even thicker by changing CQD ink concentration (Figure S13, Supporting Information). This implies that our method can produce sufficiently thick CQD films without suffering from the high-boiling-point solvent. Considering spin-coating can only produce the film with thickness up to ≈150 nm due the high-boiling-point of DMF (Figure S14, Supporting Information), our strategy can be applied to various CQD inks regardless of boiling-point of solvent (Figure S15, Supporting Information).

We compared our SSC CQD films with CQD films fabricated using the conventional solid-state LbL method. We prepared LbL-exchanged CQD films using the same MAI ligands as a form of control. Local surface roughness measured by atomic

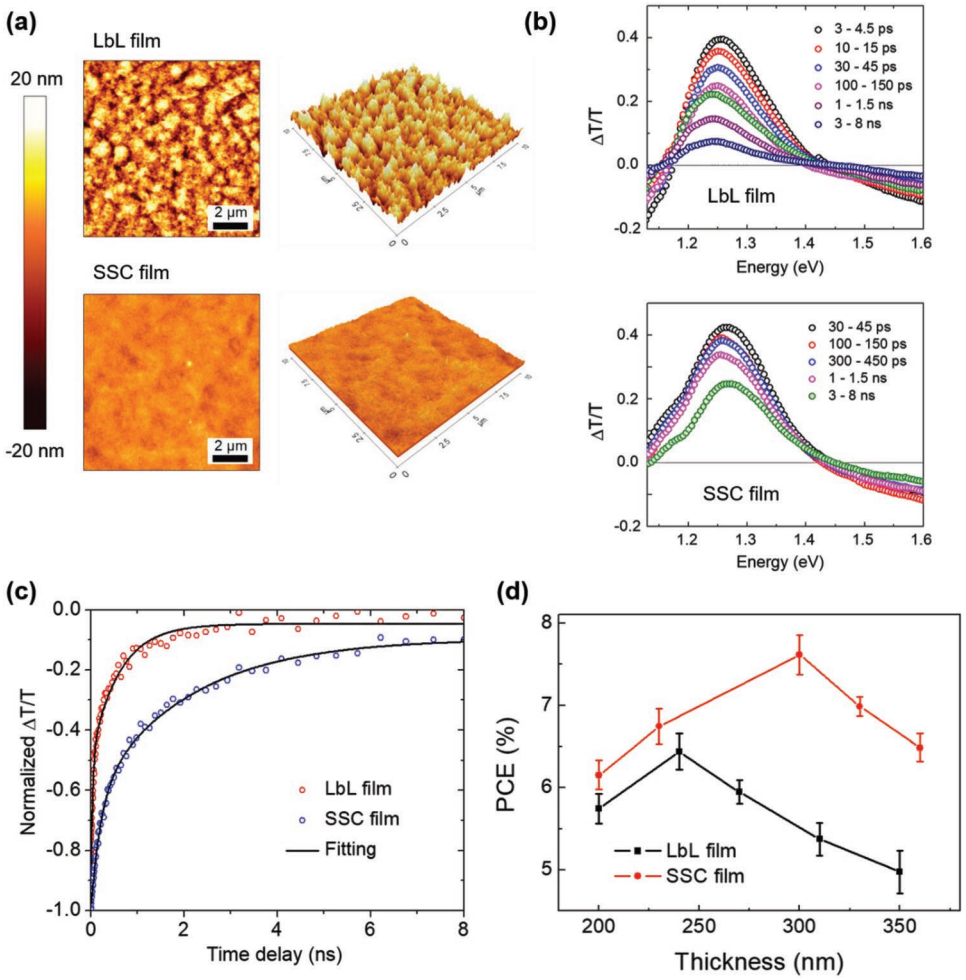

Figure 3. Comparison between the single-step spray-coating (SSC) method and conventional LbL method. a) Top and angled images of the layer-by-layer (LbL) film (top) and single-step spray-coating (SSC) film (bottom) obtained using atomic force microscopy. b) Transient absorption spectra of the LbL film (top) and the SSC film (bottom) at 700 nm. c) Ground-state bleach kinetics of the LbL film and the SSC film. The solid lines represent the best fitting to the obtained data. d) PCE of the CQD solar cells fabricated by LbL films and SSC films as a function of film thickness.

force microscopy (AFM) showed that SSC films were much smoother compared with that of LbL films (**Figure 3**a). The root-mean-square surface roughness value for the SSC film was 1.26 nm, which is much lower than 5.36 nm for the LbL film.

Time-resolved laser spectroscopy provides direct information not only about the charge carrier dynamics in real time, but also the impact of surface roughness and surface defects on the carrier recombination in CQD films. We therefore have performed femtosecond (fs) transient absorption (TA) spectroscopy for CQD films fabricated by LbL and SSC methods. The TA-experimental setup is detailed elsewhere.[42,43] In addition to the ground state bleach at 1.26 eV, due to the removal of the population from the occupied valence band, a broad absorption feature appears at higher energy. It should be noted that because we measured $\Delta T/T$, instead of the absorbance change (ΔA), the bleach peak appearing at the high-energy side can be attributed to the excited-state absorption (ESA) of the excited charge carriers.[43] Because the ground state bleach recovery of the lowest absorption peak directly reflects the depopulation of excited carriers in the band edge state (1S), we used it as a convenient marker mode to monitor the carrier dynamics of PbS CQD films fabricated by the two methods. As shown in Figures 3b,c, the change of carrier dynamics is much slower for the SSC film compared to that of the LbL film. A fast component decay time is 38 ps for the LbL film and 214 ps for the SSC film (Table S2, Supporting Information). The fast dynamics in CQDs is attributed to the trap states at the CQD surface, which lie just below the first confined electron state, resulting in fast nonradiative recombination pathways.[43–46] Thus, slow carrier dynamics in the SSC film compared to the LbL film can be evidence of reduced trap states in the SSC film. We also employed 4D scanning ultrafast electron microscopy (4D S-UEM) to map the carrier dynamics on the CQD films (Figure S16, Supporting Information). The time-resolved change in the bright contrast of the CQD film surface shows that the SSC film shows slower recombination of the excited state charge carriers compared to that of LbL film.

To confirm the charge carrier dynamics in the SSC QD films, we fabricated CQD solar cells by using the LbL film and SSC film as an active layer. The CQD films were deposited on

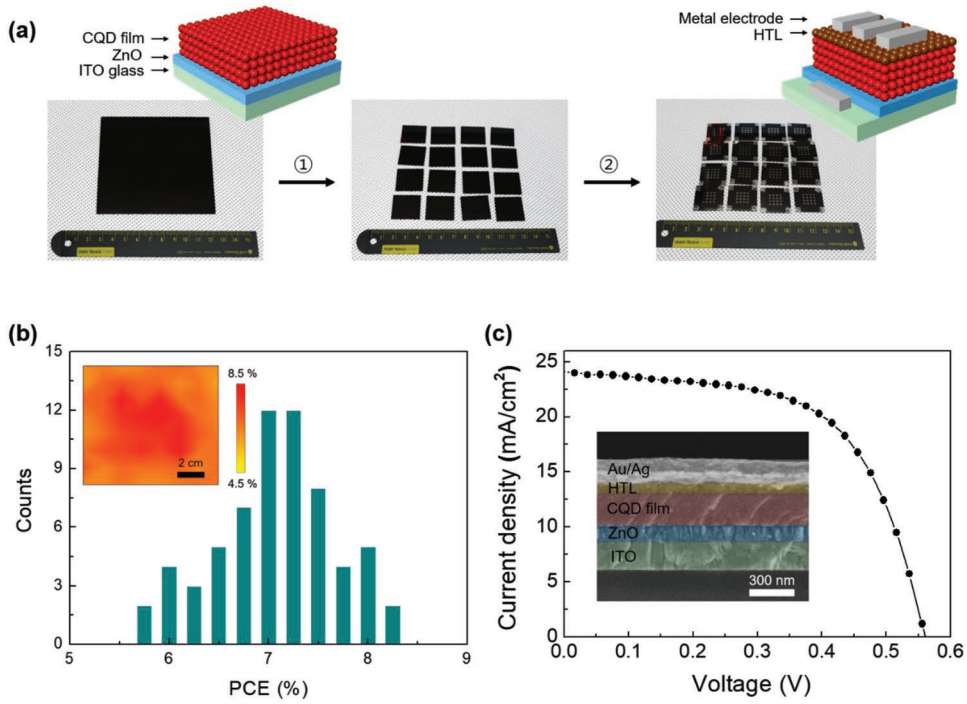

Figure 4. Scalable fabrication of CQD solar cells. a) Scheme of scalable fabrication process of CQD solar cells. Process 1: Large-area CQD films deposited on a ZnO/ITO substrate are divided into 16 parts. Process 2: Hole-transport layer (PbS CQD film treated with EDT ligand) and metal electrode are deposited on each substrate. b) Histograms of PCE from one large-area CQD substrate (100 cm^2) and their spatial map (inset). 64 PCE data from one substrate are used for statistics. c) Current density–voltage characteristics of the best-performing device. Inset image is cross-sectional SEM image of the device.

a ZnO/ITO substrate either using the LbL or the SSC method, where ZnO acts as an electron-accepting layer.[47] Two layers of 1,2-ethanedithiol-treated CQD films (≈60 nm) were deposited onto the SSC films as a hole-transporting layer (HTL).[19] For the top electrode, Au (40 nm) and Ag (120 nm) were thermally deposited to complete the device fabrication. Figure 3d shows the PCE of the devices using LbL film and SSC QD film as a function of active layer thickness. Strikingly, the device using SSC film enabled a use of thicker active layer compared to the device using LbL film, without sacrificing V_{oc} and FF. It implies the enhanced diffusion length of the CQD film, which is consistent with the slower carrier recombination rate in the SSC film compared to that of the LbL film.

We further pursued the scalable fabrication of the CQD solar cells using large-area CQD films deposited via SSC. A schematic diagram of the device fabrication process is presented in **Figure 4**a. The CQD inks were deposited on ZnO/ITO substrates (10 × 10 cm^2), then the substrate was divided into 16 parts (2.5 × 2.5 cm^2) to facilitate measurement, followed by deposition of the HTL layer and the Au/Ag top contact. Figure 4b shows statistical PCE data and their spatial map from CQD solar cells fabricated on a large-area CQD substrate (16 devices) as shown in Figure 4a, which suggests that uniform PCE output is achieved along the 10 cm x 10 cm substrate. The histogram of the device PCE collected from multiple large-area films confirms reproducibility of this process (Figure S17, Supporting Information). Figure 4c shows the cross-sectional SEM image of the CQD solar cell structure, which consists of ITO (180 nm)/ZnO (100 nm)/CQD-MAI (265 nm)/CQD-EDT (65 nm)/metal electrode (160 nm). The hero device exhibited a J_{sc} of 24.1 mA cm^{-2}, a V_{oc} of 0.56 V, a fill factor of 60%, and a PCE of 8.10% under AM1.5G conditions.

In conclusion, we demonstrate a new strategy to realize a uniform, scalable fabrication of CQD films by tuning the solute-redistribution dynamics of CQD inks with the aid of ultrasonic spray-coating system. We employed thickness profiles and XRF mapping to verify the uniformity of the film, and applied to CQD solar cells. We thereby achieve a scalable fabrication of CQD solar cells, exhibiting uniform PCE over a large area of 100 cm^2. The understanding of uniform deposition of CQD inks, which is highlighted in this work, can be widely extended to various CQD film fabrication methods for large-scale dimension.

Experimental Section

An extensive description of material synthesis, ligand exchange, film fabrication and characterization, device fabrication, and computational studies can be found in the Supporting Information.

Supporting Information

Supporting Information is available from the Wiley Online Library or from the author.

Acknowledgements

M.-J.C. and Y.K. contributed equally to this work. This work was supported by the National Research Foundation of Korea (NRF) funded by the Korea government (MSIT) (NRF-2017R1A2B2009948 and NRF-2016M3D1A1900035). This work was also supported by the KIST Institutional Program (2E27301).

Conflict of Interest

The authors declare no conflict of interest.

Keywords

colloidal quantums dot, large-area solar cells, solute redistribution

Received: September 10, 2018
Revised: April 25, 2019
Published online: May 30, 2019

[1] I. Moreels, K. Lambert, D. Smeets, D. De Muynck, T. Nollet, J. C. Martins, F. Vanhaecke, A. Vantomme, C. Delerue, G. Allan, Z. Hens, *ACS Nano* **2009**, *3*, 3023.
[2] Q. Q. Dai, Y. N. Wang, X. B. Li, Y. Zhang, D. J. Pellegrino, M. X. Zhao, B. Zou, J. Seo, Y. D. Wang, W. W. Yu, *ACS Nano* **2009**, *3*, 1518.
[3] Y. Liu, M. Gibbs, J. Puthussery, S. Gaik, R. Ihly, H. W. Hillhouse, M. Law, *Nano Lett.* **2010**, *10*, 1960.
[4] C. R. Kagan, C. B. Murray, *Nat. Nanotechnol.* **2015**, *10*, 1013.
[5] J. Song, H. Zeng, *Angew. Chem., Int. Ed.* **2015**, *54*, 9760.
[6] G. J. Supran, K. W. Song, G. W. Hwang, R. E. Correa, J. Scherer, E. A. Dauler, Y. Shirasaki, M. G. Bawendi, V. Bulovic, *Adv. Mater.* **2015**, *27*, 1437.
[7] J. Y. Kim, V. Adinolfi, B. R. Sutherland, O. Voznyy, S. J. Kwon, T. W. Kim, J. Kim, H. Ihee, K. Kemp, M. Adachi, M. J. Yuan, I. Kramer, D. Zhitomirsky, S. Hoogland, E. H. Sargent, *Nat. Commun.* **2015**, *6*, 7772.
[8] S. Kim, A. R. Marshal, D. M. Kroupa, E. M. Miller, J. M. Luther, S. Jeong, M. C. Beard, *ACS Nano* **2015**, *9*, 8157.
[9] M. J. Choi, J. Oh, J. K. Yoo, J. Choi, D. M. Sim, Y. S. Jung, *Energy Environ. Sci.* **2014**, *7*, 3052.
[10] J. Choi, Y. Kim, J. W. Jo, J. Kim, B. Sun, G. Walters, F. P. G. de Arquer, R. Quintero-Bermudez, Y. Y. Li, C. S. Tan, L. N. Quan, A. P. T. Kam, S. Hoogland, Z. H. Lu, O. Voznyy, E. H. Sargent, *Adv. Mater.* **2017**, *29*, 1702350.
[11] J. W. Jo, Y. Kim, J. M. Choi, F. P. G. de Arquer, G. Walters, B. Sun, O. Ouellette, J. W. Kim, A. H. Proppe, R. Quintero-Bermudez, J. Fan, J. X. Xu, C. S. Tan, O. Voznyy, E. H. Sargent, *Adv. Mater.* **2017**, *29*, 1703627.
[12] Z. Y. Yang, J. Z. Fan, A. H. Proppe, F. P. G. de Arquer, D. Rossouw, O. Voznyy, X. Z. Lan, M. Liu, G. Walters, R. Quintero-Bermudez, B. Sun, S. Hoogland, G. A. Botton, S. O. Kelley, E. H. Sargent, *Nat. Commun.* **2017**, *8*, 1325.
[13] J. H. Song, H. Choi, Y. H. Kim, S. Jeong, *Adv. Energy Mater.* **2017**, *7*, 1700301.
[14] T. Chiba, Y. Hayashi, H. Ebe, K. Hoshi, J. Sato, S. Sato, Y.-J. Pu, S. Ohisa, J. Kido, *Nat. Photonics* **2018**, *12*, 681.
[15] H. C. Wang, Z. Bao, H. Y. Tsai, A. C. Tang, R. S. Liu, *Small* **2018**, *14*, 1702433.
[16] Q. S. Shan, J. H. Li, J. Z. Song, Y. S. Zou, L. M. Xu, J. Xue, Y. H. Dong, C. X. Huo, J. W. Chen, B. N. Han, H. B. Zeng, *J. Mater. Chem. C* **2017**, *5*, 4565.
[17] J. Song, T. Fang, J. Li, L. Xu, F. Zhang, B. Han, Q. Shan, H. Zeng, *Adv. Mater.* **2018**, *30*, 1805409.
[18] M. X. Liu, O. Voznyy, R. Sabatini, F. P. G. de Arquer, R. Munir, A. H. Balawi, X. Z. Lan, F. J. Fan, G. Walters, A. R. Kirmani, S. Hoogland, F. Laquai, A. Amassian, E. H. Sargent, *Nat. Mater.* **2017**, *16*, 258.
[19] C. H. M. Chuang, P. R. Brown, V. Bulovic, M. G. Bawendi, *Nat. Mater.* **2014**, *13*, 796.
[20] A. Fischer, L. Rollny, J. Pan, G. H. Carey, S. M. Thon, S. Hoogland, O. Voznyy, D. Zhitomirsky, J. Y. Kim, O. M. Bakr, E. H. Sargent, *Adv. Mater.* **2013**, *25*, 5742.
[21] D. N. Dirin, S. Dreyfuss, M. I. Bodnarchuk, G. Nedelcu, P. Papagiorgis, G. Itskos, M. V. Kovalenko, *J. Am. Chem. Soc.* **2014**, *136*, 6550.
[22] Z. J. Ning, H. P. Dong, Q. Zhang, O. Voznyy, E. H. Sargent, *ACS Nano* **2014**, *8*, 10321.
[23] H. T. Zhang, B. Hu, L. F. Sun, R. Hovden, F. W. Wise, D. A. Muller, R. D. Robinson, *Nano Lett.* **2011**, *11*, 5356.
[24] S. Kim, J. Noh, H. Choi, H. Ha, J. H. Song, H. C. Shim, J. Jang, M. C. Beard, S. Jeong, *J. Phys. Chem. Lett.* **2014**, *5*, 4002.
[25] H. Choi, J. G. Lee, X. D. Mai, M. C. Beard, S. S. Yoon, S. Jeong, *Sci. Rep.* **2017**, *7*, 622.
[26] C. Girotto, D. Moia, B. P. Rand, P. Heremans, *Adv. Funct. Mater.* **2011**, *21*, 64.
[27] K. Hwang, Y. S. Jung, Y. J. Heo, F. H. Scholes, S. E. Watkins, J. Subbiah, D. J. Jones, D. Y. Kim, D. Vak, *Adv. Mater.* **2015**, *27*, 1241.
[28] X. Z. Lan, O. Voznyy, A. Kiani, F. P. G. de Arquer, A. S. Abbas, G. H. Kim, M. X. Liu, Z. Y. Yang, G. Walters, J. X. Xu, M. J. Yuan, Z. J. Ning, F. J. Fan, P. Kanjanaboos, I. Kramer, D. Zhitomirsky, P. Lee, A. Perelgut, S. Hoogland, E. H. Sargent, *Adv. Mater.* **2016**, *28*, 299.
[29] Y. F. Li, Y. J. Sheng, H. K. Tsao, *Langmuir* **2013**, *29*, 7802.
[30] Y. N. Li, Q. Yang, M. Z. Li, Y. L. Song, *Sci. Rep.* **2016**, *6*, 24628.
[31] B. M. Weon, J. H. Je, *Phys. Rev. Lett.* **2013**, *110*, 028303.
[32] Y. Tsoumpas, S. Dehaeck, A. Rednikov, P. Colinet, *Langmuir* **2015**, *31*, 13334.
[33] J. Park, J. Moon, *Langmuir* **2006**, *22*, 3506.
[34] T. P. Bigioni, X. M. Lin, T. T. Nguyen, E. I. Corwin, T. A. Witten, H. M. Jaeger, *Nat. Mater.* **2006**, *5*, 265.
[35] C. Jiang, Z. Zhong, B. Liu, Z. He, J. Zou, L. Wang, J. Wang, J. Peng, Y. Cao, *ACS Appl. Mater. Interfaces* **2016**, *8*, 26162.
[36] H. Aqoma, S. Y. Jang, *Energy Environ. Sci.* **2018**, *11*, 1603.
[37] X. Yang, C. Y. Li, Y. Sun, *Soft Matter* **2014**, *10*, 4458.
[38] T. Z. Qian, X. P. Wang, P. Sheng, *J. Fluid Mech.* **2006**, *564*, 333.
[39] M. Doi, *J. Phys.: Condens. Matter* **2011**, *23*, 284118.
[40] R. D. Deegan, O. Bakajin, T. F. Dupont, G. Huber, S. R. Nagel, T. A. Witten, *Nature* **1997**, *389*, 827.
[41] X. Man, M. Doi, *Phys. Rev. Lett.* **2016**, *116*, 066101.
[42] A. O. El-Ballouli, E. Alarousu, M. Bernardi, S. M. Aly, A. P. Lagrow, O. M. Bakr, O. F. Mohammed, *J. Am. Chem. Soc.* **2014**, *136*, 6952.
[43] A. O. El-Ballouli, E. Alarousu, A. Usman, J. Pan, O. M. Bakr, O. F. Mohammed, *ACS Photonics* **2014**, *1*, 285.
[44] V. Sukhovatkin, S. Hinds, L. Brzozowski, E. H. Sargent, *Science* **2009**, *324*, 1542.
[45] A. Jain, O. Voznyy, M. Korkusinski, P. Hawrylak, E. H. Sargent, *J. Phys. Chem. Lett.* **2017**, *8*, 3179.
[46] A. El-Ballouli, E. Alarousu, A. R. Kirmani, A. Amassian, O. M. Bakr, O. F. Mohammed, *Adv. Funct. Mater.* **2015**, *25*, 7435.
[47] M. J. Choi, S. Kim, H. Lim, J. Choi, D. M. Sim, S. Yim, B. T. Ahn, J. Y. Kim, Y. S. Jung, *Adv. Mater.* **2016**, *28*, 1780.